Dihydrogen Bonding in Compressed Ammonia Borane and Its Roles in Structural Stability

ARTICLE *in* THE JOURNAL OF PHYSICAL CHEMISTRY C · NOVEMBER 2014

Impact Factor: 4.77 · DOI: 10.1021/jp509633h

4 AUTHORS, INCLUDING:

Xue Yong
University of Saskatchewan
5 PUBLICATIONS **44** CITATIONS
SEE PROFILE

John S Tse
University of Saskatchewan
597 PUBLICATIONS **11,757** CITATIONS
SEE PROFILE

Michael Greschner
University of Saskatchewan
2 PUBLICATIONS **1** CITATION
SEE PROFILE

THE JOURNAL OF PHYSICAL CHEMISTRY C

Article

pubs.acs.org/JPCC

Dihydrogen Bonding in Compressed Ammonia Borane and Its Roles in Structural Stability

Yansun Yao,*[,†,‡] Xue Yong,[†] John S. Tse,[†] and Michael J. Greschner[†,‡]

[†]Department of Physics and Engineering Physics, University of Saskatchewan, Saskatoon, Saskatchewan S7N 5E2, Canada

[‡]Canadian Light Source, Saskatoon, Saskatchewan S7N 2V3, Canada

Supporting Information

ABSTRACT: Theoretical structure prediction calculations have revealed that the conformation of ammonia borane (NH_3BH_3) in the crystalline state can be modified by pressure, changing from the staggered configuration at low pressure to an eclipsed geometry at high pressure. At low pressure, the crystalline structure is stabilized by the charge transfer N—$H^{\delta+}$···$^{\delta-}$H—B dihydrogen interactions. In the high pressure polymorphs, the NH_3BH_3 is predicted to form a layered structure. The N—$H^{\delta+}$···$^{\delta-}$H—B bonding is still predominant within the layer. The stacking of the layers, however, is determined by the occurrence of additional homopolar B—$H^{\delta-}$···$^{\delta-}$H—B interaction unprecedented in NH_3BH_3 and facilitated by the eclipsed conformation. This bonding is shown to be the result of secondary interactions between BH_3 groups from molecules of adjacent layers. Topological analysis of the charge density and perturbation calculations on the molecule fragments show unambiguously that the B—$H^{\delta-}$···$^{\delta-}$H—B interaction is covalent in nature with the bond strength comparable to a conventional hydrogen bond.

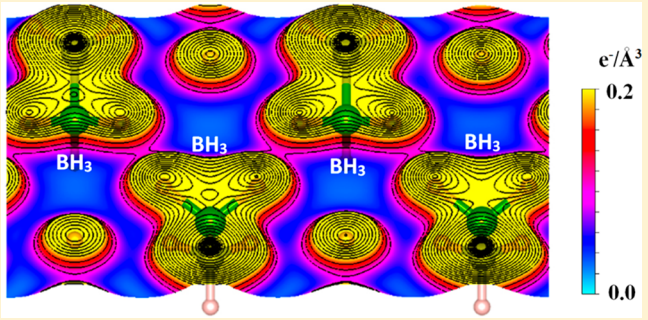

INTRODUCTION

Hydrogen, the most abundant element in the universe, is a promising candidate to eventually replace petroleum as the fuel of choice. In the context of hydrogen storage research, ammonia borane (NH_3BH_3) has received continuous attention for decades due to its high storage capacity and moderate dehydrogenation temperature. Molecular NH_3BH_3 is a prototypical electron donor−acceptor complex formed between NH_3 and BH_3 molecules (**1**) and arranged in a staggered conformation similar to the geometry of the isoelectronic ethane (C_2H_6). In solid state, however, NH_3BH_3 and C_2H_6 have very different physical properties. For example, the melting temperature of NH_3BH_3 is higher than that of C_2H_6 by 285 K. This suggests a strong intermolecular interaction, often referred to as "dihydrogen bonding" (**2**),[1−3] to present in NH_3BH_3. The dihydrogen bonding originates from the N—$H^{\delta+}$···$^{\delta-}$H—B charge-transfer interaction which usually occurs when the intermolecular distance $d_{H\cdots H}$ is shorter than the sum of the van der Waals (vdW) radii. A survey of the Cambridge Structural Database (CSD) carried out by Richardson et al.[2] shows that dihydrogen bonding has a preference for a bent B—H···HN angle θ and a nearly linear N—H···HB angle ψ, arranged such that the N—H vector points toward the middle of the B—H vector. This geometry suggests that the electron donor of the dihydrogen bond is the B—H σ bond, rather than an individual atom. This is an extraordinary illustration of the versatility of the hydrogen bonding; in the past, we have seen π electrons of a multiple bond or aromatic ring, or a transition metal center, act as electron donors.[4,5]

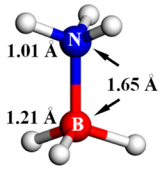

1

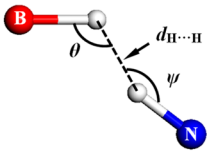

2

Clearly, dihydrogen bonding, to a great extent, determines the crystal structures of NH_3BH_3. At ambient conditions, NH_3BH_3 adopts a dynamical disordered structure (*I*4*mm*), which exhibits halos of hydrogen atom occupancy surrounding the N and B atoms.[6,7] Below 225 K, NH_3BH_3 has an ordered phase[8] with fixed hydrogen positions (*Pmn*2$_1$). Upon an increase in pressure, the Raman spectra of NH_3BH_3 show a redshift in the N—H stretching mode and a blueshift in the B—H stretching mode,[9−12] indicating a strengthening of the dihydrogen bond via enhanced charge transfer (δ). X-ray diffraction measurements assisted by ab initio calculations have established the crystal structures of two high-pressure phases. An ordered *Cmc*2$_1$ structure[13,14] is found to be stable above 1.0 GPa at room temperature. Upon heating, the *Cmc*2$_1$ structure

Received: September 23, 2014
Revised: November 18, 2014
Published: November 25, 2014

   dx.doi.org/10.1021/jp509633h | *J. Phys. Chem. C* 2014, 118, 29591−29598

transforms to a proton-disordered *Pnma* structure.[15] Infrared measurement, Raman spectroscopy, X-ray and neutron diffractions, as well as molecular dynamics (MD) simulations have provided evidence that there are other stable phases of NH_3BH_3 at high pressure.[16−21]

This paper reports a theoretical study on the high-pressure structures of NH_3BH_3. Two new crystalline structures, with space groups *Ama*2 and $P2_1/m$ as stable phases under high pressure, were predicted. The *Ama*2 structure is calculated to be more stable than all previously reported NH_3BH_3 structures above 5.8 GPa, while the $P2_1/m$ structure becomes more stable than the *Ama*2 structure above 25 GPa. Remarkably, all NH_3BH_3 molecules in the predicted structures adopt an unprecedented eclipsed conformation, which is stabilized under high pressure by dihydrogen interactions. To investigate the details of the dihydrogen bonding, the local environment of the NH_3BH_3 molecules in the solid is characterized by a variety of theoretical techniques, including the quantum theory of atoms-in-molecules (QTAIM),[22] natural bond orbital (NBO),[23] Wiberg bond index (WBI),[24] and charge decomposition analysis (CDA).[25] The results confirm the primary role of dihydrogen bonding in stabilizing the solid structures. A significant finding is the identification of a subtle B—$H^{\delta-}\cdots^{\delta-}$H—B interaction between hydrogen atoms of the same polarity. This interaction helps to stabilize the otherwise unfavorable eclipse conformation and becomes progressively important under high pressure. The outline of this paper is as follows. First, the structure and bonding of solid NH_3BH_3 phases at ambient pressure are discussed. The purpose is to examine the role of the heteropolar N—$H^{\delta+}\cdots^{\delta-}$H—B bonding in the solid state. Next, the effect of pressure on the conformation of the NH_3BH_3 molecules in the crystals is presented. The occurrence of the homopolar B—$H^{\delta-}\cdots^{\delta-}$H—B bonding are characterized. Finally, the relative importance of the heteropolar and homopolar bonding in the stabilization of the crystal and molecular structures is discussed.

METHODS

To identify the low-energy crystal structures of NH_3BH_3, we employed a structure search scheme to locate the energy minima through an exhaustive scan of the energy surface by numerous trials. This method has been applied successfully in the past for the determination the high-pressure phase of ammonium borohydride (NH_4BH_4).[26] Trial crystal structures were constructed from random distributions of either staggered or eclipsed NH_3BH_3, using the molecular structures optimized in gas phase. For each molecule type, 200 different stacking patterns were generated randomly in unit cells of arbitrary shapes that contain up to four molecules. The orientations of the molecules are also randomized in the unit cell. The geometries of all the trial structures were then fully optimized. Those with the lowest enthalpies were then annealed to 300 K and equilibrated for 10 ps, in a 2 × 2 × 2 supercell, using ab initio MD calculations in a microcanonical (NVT) ensemble. This is followed by a second structural optimization. The purpose of the annealing step is to ensure that the crystalline structure indeed reaches an energy minimum as, occasionally, new structures were found after annealing.[27]

Geometry optimization, enthalpies, and phonon band structures were calculated using first-principles electronic structure methods based on the density-functional theory (DFT). Electronic and MD calculations were performed with the Vienna ab initio simulation program (VASP).[28] The projector-augmented planewave (PAW) potential[29,30] treats the 2*s* and 2*p* orbitals as valence levels for N and B atoms with the Perdew−Burke−Ernzerhof (PBE) exchange-correlation functional.[31] The wave functions are expanded in a planewave basis set with an energy cutoff of 700 eV. Dense *k*-point meshes were employed to sample the first Brillouin zone (BZ) to ensure the energies converged to better than 1 meV/atom. Phonon band structures were calculated using the ABINIT program,[32] employing the Troullier−Martins pseudopotentials,[33,34] the PBE functional, and an energy cutoff of 80 Ry. The interatomic force constant matrix was calculated using linear response method in a 4 × 4 × 4 *q*-point mesh and an 8 × 8 × 8 *k*-point mesh. The all-electron charge density was computed in a 60 × 60 × 60 grid of the unit cell using the VASP program. Topological analysis of the charge density was carried out using the InteGrity program[35] based on the QTAIM. The AIM theory is an extension of quantum mechanics to open systems in which an atom within a solid is defined through the "zero-flux" condition of the electron density gradient $\nabla\rho(\boldsymbol{r})$. The electron density distribution $\rho(\boldsymbol{r})$ and its curvatures at the saddle point along a bond path, often referred to as the "bond critical point", provides information about the electron concentration in the interatomic regions, which correlate closely to the type and properties of bonding. The AIM theory has been applied with great success for the characterization of a variety of systems, such as ionic, covalent, or hydrogen-bonded compounds.[36−38] The NBO and WBI calculations were performed using the Gaussian 09 suite program,[39] employing the PBE1PBE density functional and 6-31G(d) basis sets. The Multiwfn program[40] was used to perform CDA and extended charge decomposition analysis (ECDA). Structures and orbitals presented in the figures were prepared with the VESTA program[41] and the VMD program.[42]

RESULTS AND DISCUSSION

Solid Ammonia Borane at Ambient Pressure. Crystalline structures of NH_3BH_3 at 1 atm were constructed in two groups consist of either solely staggered or eclipsed molecules. The $Pmn2_1$ structure (Figure 1a) observed experimentally at low temperatures[8] was found to have the lowest energy among all structures examined. This structure was found to be more stable than the lowest energy structure that contains only eclipsed molecules, by about 2.6 kcal/mol. Coincidentally, this energy difference is almost identical to the energy difference between two molecular conformers.[43] In the $Pmn2_1$ structure, each NH_3BH_3 molecule is linked to four nearest-neighbor molecules and four second-nearest-neighbor molecules in a head-to-tail fashion through N—$H^{\delta+}\cdots^{\delta-}$H—B bonds (Figure 1b). These dihydrogen bonds are arranged in layers perpendicular to the *c*-axis; one such layer is depicted in Figure 1c. Within the layer all NH_3 and BH_3 groups have identical orientations. The neighboring layers above or below would have been identical, but since the molecules are staggered, they must have the N—H and B—H bonds pointing in the opposite directions. A QTAIM analysis has identified the locations of the bond critical points in the crystal (Figure 1b,c). The shortest H···H contact (1.89 Å) was found in a pair of bonds, N2—H···H—B1 and N3—H···H—B1, which has a bent ∠B—H···HN (100°) and a nearly linear ∠N—H···HB (161°). Both features are close to the expected ideal geometry described above (vide infra). The second shortest H···H contact (2.07 Å) was found in another pair, N4—H···H—B1 and N5—H···H—B1, which however has a nearly linear ∠B—H···HN (158°) and a bent

dx.doi.org/10.1021/jp509633h | J. Phys. Chem. C 2014, 118, 29591−29598

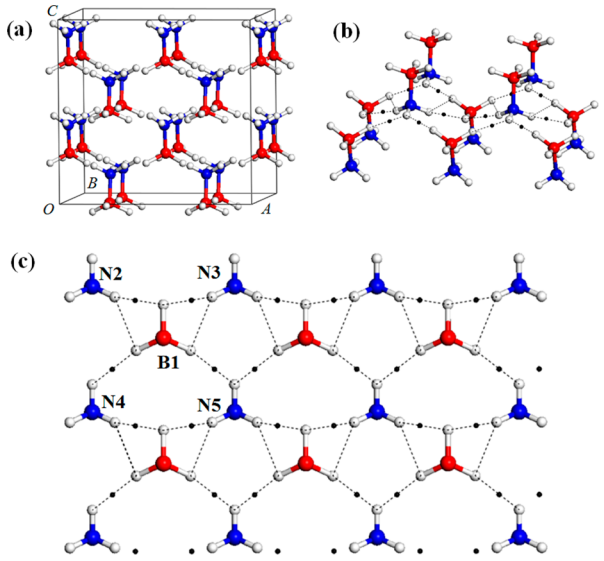

Figure 1. (a) The $Pmn2_1$ structure shown in a 2 × 2 × 2 supercell. Network of intermolecular H···H contacts (dashed lines) shown (b) in an extended structure and (c) on a plane perpendicular to the *c*-axis. Nitrogen, boron, and hydrogen atoms are colored in blue, red, and white, respectively. Positions of the bond critical points are indicated by black dots.

∠N—H···HB (128°). The occurrence of the two types of dihydrogen geometry is due to the fact that, in the solid state, it is not possible to arrange all the dihydrogen bonds in the same, preferred manner. QTAIM calculated charge densities at the bond critical points for the two H···H contacts are 0.84 and 0.45 e^{-}·$Å^{-3}$, respectively, confirming that the shorter bonds are indeed stronger. Furthermore, even though the geometries are different, both dihydrogen bonds have small but positive Laplacians, a characteristic of the closed-shell interactions.[44,45] The *I*4*mm* structure observed at above 225 K is a hydrogen disordered phase.[6,7] Since the hydrogen positions cannot be uniquely defined, we have not calculated the energy of this structure. It is expected that the *I*4*mm* structure should have energy comparable to that of the $Pmn2_1$ structure. Due to the rotating NH_3 and BH_3 groups, the dihydrogen bonding environment is not able to be unambiguously characterized in this structure.

Crystalline Structures of Ammonia Borane at High Pressure: Earlier Studies. Spectroscopic studies have revealed at least three consecutive structural transitions of NH_3BH_3 upon compression to 20 GPa. At room temperature, two phase transitions were identified by X-ray diffraction experiments. The first phase transition near 1.5 GPa is well established, where the *I*4*mm* structure transforms to an orientational ordered $Cmc2_1$ structure.[13,14] In the $Cmc2_1$ structure, all NH_3BH_3 molecules have a staggered conformation. The second phase transition was observed close to 12.9 GPa, and the new phase was suggested to have a $P2_1$ space group and may consist of both types of molecular conformers.[20] At elevated temperatures, the $Cmc2_1$ structure undergoes a transition to a hydrogen disordered *Pnma* phase.[15] A separate X-ray diffraction study[17] shows that a structure with very low *P*1 symmetry may exist above 8 GPa. Recent MD simulations[18] also suggest two model structures, both with the $P2_1$ space group, to become stable at 15 and 25 GPa, respectively. Furthermore, a recent Raman spectroscopic measurement up to 65 GPa[12] reported a phase transition at 27 GPa, although the structure of this new phase remains elusive. Previous high-pressure studies of NH_3BH_3 and their implications to hydrogen storage applications have recently reviewed by Song.[46]

Ammonia Borane under Pressure: Interplay of Molecular Conformation and Dihydrogen Bonding. Crystalline structures built from either staggered or eclipsed NH_3BH_3 molecules were investigated at high pressures. In Figure 2, the enthalpies of three predicted low-energy

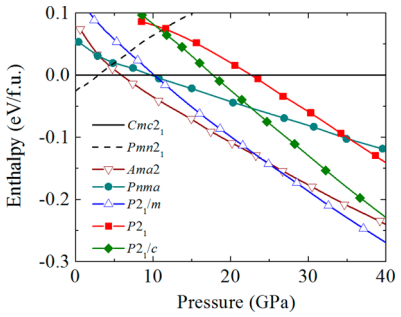

Figure 2. Calculated pressure dependences of enthalpies for selected NH_3BH_3 solid structures, relative to the $Cmc2_1$ structure.

structures with the *Ama*2, $P2_1/m$, and $P2_1/c$ space groups are compared with those of the experimentally known $Pmn2_1$, $Cmc2_1$, and *Pnma* structures, and that of the theoretically predicted $P2_1$ structure,[18] in the pressure range of 0−40 GPa. The alternative $P2_1$ structure[20] was found to be mechanically unstable and energetically noncompetitive in this pressure range and will not be discussed here.

Figure 2 shows that the $Cmc2_1$ structure becomes more stable than the $Pmn2_1$ structure at *c.* 2.8 GPa, which compares well with the experimental transition pressure of 1.5 GPa (measured at $T \approx 180$ K).[13] At 9.6 GPa, the *Pnma* structure is predicted to become more stable than the $Cmc2_1$ structure. Experimentally, the *Pnma* structure has only been studied under high-temperature conditions, i.e., 380 K and upward.[15] Therefore, it is not straightforward to make a direct comparison of the relative stability of the two phases from athermal calculations; an explicit consideration of entropic effect is needed. Nevertheless, X-ray diffraction measurements had revealed that the *Pnma* structure became stable and coexisted with the $Cmc2_1$ structure at high temperature near 5.5 GPa, in close agreement with the calculations. It is important to note that both the $Cmc2_1$ and *Pnma* structures contain entirely the staggered molecules (see Supporting Information, SI). In the $Cmc2_1$ structure, each NH_3BH_3 molecule is connected to 10 neighbors, through 12 N—$H^{\delta+}$···$^{\delta-}$H—B dihydrogen bonds, four of which are bifurcated. Similar to the zero-pressure high-temperature *I*4*mm* structure, the *Pnma* structure is also a hydrogen-disordered rotor phase. The positions of hydrogen atoms used in the enthalpy calculations were obtained from the optimized static geometry. Clearly, the structural motifs of the $Cmc2_1$ and *Pnma* structures are similar to their corresponding ambient-pressure counterparts, $Pmn2_1$ and *I*4*mm* structures, respectively.

Near 6 GPa, a structure consisting of only eclipsed NH_3BH_3 molecules with the *Ama*2 space group is found to be thermodynamically most stable (Figure 2). This structure was predicted to transform to a $P2_1/m$ phase, also made up of eclipsed molecules, at *c.* 23.9 GPa. In this pressure range, structures containing staggered molecules are higher in enthalpy when compared to these two structures. Calculated

dx.doi.org/10.1021/jp509633h | J. Phys. Chem. C 2014, 118, 29591−29598

phonon band structures (see SI) for both structures show no imaginary frequencies, indicating that both structures are mechanically stable. The optimized structural parameters for the *Ama*2 and the $P2_1/m$ structures are listed in SI. It is interesting, and significant, that theoretical calculations predict that NH_3BH_3 adopts an eclipsed conformation in solid state once sufficient pressure is applied. As a well-known fact, the staggered conformer is intrinsically lower in energy than the eclipsed one.[47] Compression will certainly have an effect on the molecular geometry; molecules in the crystals are expected to be distorted. However, it is unlikely that the energy involved in the small distortions can compensate for the reversal of the order of the molecular stability. To illustrate this point, we have extracted an eclipsed molecule from the *Ama*2 structure and a staggered molecule from the $Cmc2_1$ structure, and compared their energy difference, which turns out to be *c.* 0.09 eV/f.u., almost the same as the energy difference between undistorted molecules.[43] Clearly, the stabilization of eclipsed molecules in high-pressure crystals must come from a different origin. We can thus show that a new type of dihydrogen interaction helps in overcoming the energetic disadvantages of the eclipsed conformation, and that the stacking of the molecules in the crystal plays a key role.

As an explicit example, we shall study the crystal and electronic structures of the high-pressure *Ama*2 phase (Figure 3a) in detail. The $P2_1/m$ structure has a very similar bonding

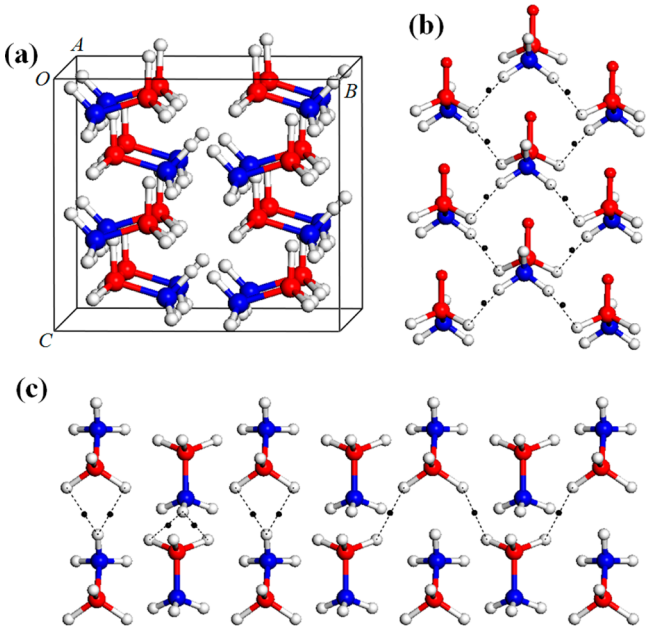

Figure 3. (a) The *Ama*2 structure shown in a 2 × 2 × 2 supercell. (b) Network of the shortest intermolecular H···H contacts. (c) Network of the second shortest (left half) and the third shortest (right half) intermolecular H···H contacts. Bond critical points are indicated by black dots.

motif; a discussion is provided in SI. In the *Ama*2 structure, NH_3BH_3 molecules form slabs parallel to the ***a*–*c*** plane; one such slab is shown in Figure 3b. Within each slab, the molecules are connected to four nearest neighbors in a head-to-tail fashion via dihydrogen bonds. As a result of these interactions, the N—B bonds are tilted toward their nearest neighbors. The dihydrogen bonds are arranged in two layers, and, since the molecules are eclipsed, these two layers have identical geometry. This configuration, therefore, allows all four equivalent N—$H^{\delta+}$···$^{\delta-}$H—B bonds connected to a molecule to have a bent ∠B—H···HN (101.45°) and a nearly linear ∠N—H···HB (161.35°), which is the preferred geometry for the N—$H^{\delta+}$···$^{\delta-}$H—B bond (vide infra). In Figure 4a, the all-

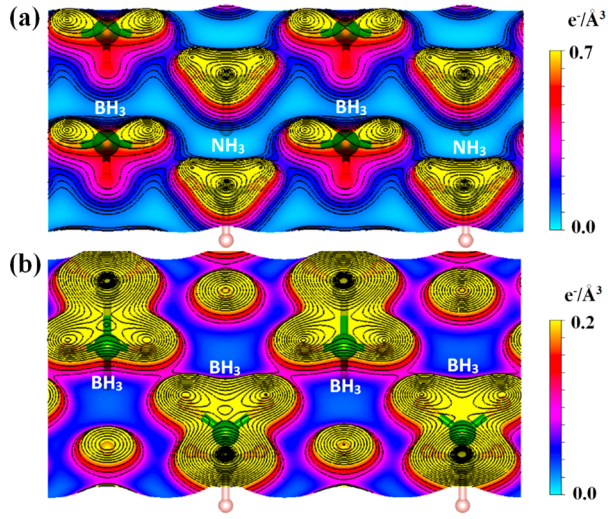

Figure 4. All-electron density maps for (a) the shortest N—$H^{\delta+}$···$^{\delta-}$H—B contacts within a slab and (b) the shortest B—$H^{\delta-}$···$^{\delta-}$H—B contacts across adjacent slabs, in the *Ama*2 structure optimized at 10 GPa.

electron density map depicted on one of these layers shows unambiguously an accumulation of electrons between the NH_3 and BH_3 groups. When two NH_3BH_3 molecules are brought close to each other, electrons from the two molecular fragments are pushed into the intermolecular regions to compensate for the unfavorable interproton repulsions.[48] The dihydrogen bonding network originates from these accumulated electron densities. A more quantitative analysis from the examination of the bond critical points will be presented later (vide supra). The N—$H^{\delta+}$···$^{\delta-}$H—B bonds in the slabs have short H···H contacts, i.e., 1.60 Å (at 10 GPa), which is significantly shorter than the vdW separation (2.40 Å). In comparison, at the same pressure the shortest H···H contacts in the $Cmc2_1$ structure and the *Pnma* structure are 1.73 and 1.85 Å, respectively.

The adjacent slabs in the *Ama*2 structure are also linked by dihydrogen interactions. The interactions have two types: bifurcated N—$H^{\delta+}$···$^{\delta-}$H—B bond and homopolar B—$H^{\delta-}$···$^{\delta-}$H—B bond (Figure 3c). The bifurcated bonding features two equivalent H···H bonds involving one hydrogen atom from NH_3 and two hydrogen atoms from BH_3. The calculated H···H distance is 1.96 Å, notably longer than those within the slabs. The ∠N—H···HB and ∠B—H···HN are 149.48° and 97.63°, respectively. A similar bifurcated geometry has been suggested[49] for the head-to-tail $(NH_3BH_3)_2$ dimer. The calculated H···H distance of 1.99 Å, ∠N—H···HB of 144.48°, and ∠B—H···HN of 88.6°, for the dimer are comparable to those in the *Ama*2 solid. Significantly, the homopolar B—$H^{\delta-}$···$^{\delta-}$H—B interaction also appears to participate in stabilizing the eclipsed conformers in the crystal. The homopolar bond has a symmetric geometry, i.e., the B—H bond lengths and the B—H···HB angles are equal for both molecular fragments. This geometrical arrangement is a result of a secondary covalent interaction, which can be explained, in part, through molecular orbital theory. Such a feature therefore

dx.doi.org/10.1021/jp509633h | J. Phys. Chem. C 2014, 118, 29591−29598

Table 1. Topological Properties of the Bond Critical Points at the Three Shortest Intermolecular H···H Contacts for the *Ama*2 and $Cmc2_1$ Structures at 10 GPa[a]

structure	d (Å)	bond type	multiplicity	$\rho(r_{BCP})$ ($e^-\cdot Å^{-3}$)	$\nabla^2\rho(r_{BCP})$ ($e^-\cdot Å^{-5}$)	E_{BD}(kJ·mol^{-1})
*Ama*2	1.60	N—H$^{\delta+}$···$^{\delta-}$H—B	4	0.2186	1.4435	31.367
	1.96	N—H$^{\delta+}$···$^{\delta-}$H—B	4	0.1099	1.1495	13.106
	2.03	B—H$^{\delta-}$···$^{\delta-}$H—B	4	0.1039	0.8314	10.957
$Cmc2_1$	1.73	N—H$^{\delta+}$···$^{\delta-}$H—B	4	0.1621	1.4809	21.798
	1.76	N—H$^{\delta+}$···$^{\delta-}$H—B	4	0.1363	1.4053	17.672
	1.89	N—H$^{\delta+}$···$^{\delta-}$H—B	4	0.1294	1.2193	15.891

[a]Multiplicity is the number of dihydrogen bonds connected to a NH_3BH_3 molecule.

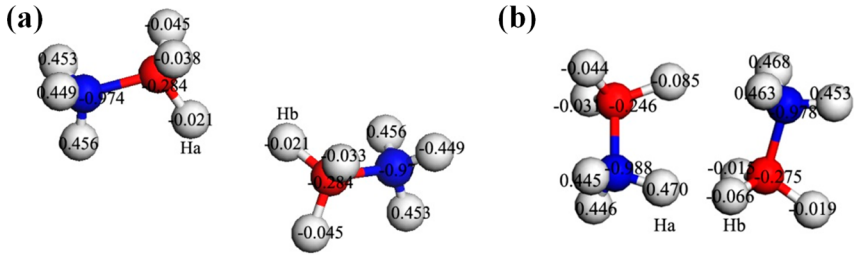

Figure 5. $(NH_3BH_3)_2$ dimers extracted from the *Ama*2 structure optimized at 10 GPa. (a) A tail-to-tail dimer linked by a B—H$^{\delta-}$···$^{\delta-}$H—B bond. (b) A head-to-tail dimer linked by a N—H$^{\delta+}$···$^{\delta-}$H—B bond. Nitrogen, boron, and hydrogen atoms are colored in blue, red, and white, respectively. Numbers displayed on the atoms are the values of the NBO charges.

separates the B—H$^{\delta-}$···$^{\delta-}$H—B interaction from the vdW interactions which are nondirectional in nature. At 10 GPa, the calculated ∠B—H···HB angle and H···H distance for the homopolar interaction are 139.39° and 2.03 Å, respectively. Clearly, this H···H distance is still much shorter than the sum of two vdW radii. The calculated all-electron density map shows an accumulation of electrons, albeit with lower densities, between two homopolar hydrogen atoms (Figure 4b). A characterization of this interaction is made in the SI, using a Hirshfeld surface analysis. The homopolar dihydrogen interaction has been observed previously in a wide variety of organic and organometallic molecules; a review of this is given in ref 50. The B—H$^{\delta-}$···$^{\delta-}$H—B interaction was predicted to present in $(NH_3BH_3)_4$ tetramers.[51] Experimental evidence of this interaction have been revealed in the thermal decomposition process of NH_3BH_3.[52] Similar interactions also present in alkali-metal amido-boranes[53] and potentially can play a key role in hydrogen storage applications. The homopolar C—H···H—C interactions have been observed in alkanes.[54,55]

In Table 1, the topological properties of the electron density in the *Ama*2 structure are presented and compared with those in the $Cmc2_1$ structure. This comparison reveals a general "shorter bond = stronger bond" paradigm. The electron density $\rho(r_{BCP})$ at the bond critical point is directly determined by the H···H distance d; the relation is almost linear, and independent of the bond polarities. For conventional hydrogen bonds, earlier ambient pressure studies[36,37] suggest that the $\rho(r_{BCP})$ should fall in a range of 0.04 to 0.24 $e^-\cdot Å^{-3}$. By this approximate measure all dihydrogen interactions in solid NH_3BH_3 may be comparable in strength to that of conventional hydrogen bonds. Notably, the intraslab N–H$^{\delta+}$···$^{\delta-}$H–B bonds (1.60 Å) in the *Ama*2 structure appear to be on the stronger side of this category. The Laplacian $\nabla^2\rho(r_{BCP})$ at the bond critical point, $\nabla^2\rho(r_{BCP})$, identifies the ionicity of the bond. For closed-shell interactions, the $\nabla^2\rho(r_{CP})$ is positive and its magnitude decreases from ionic bonding to hydrogen bonding, and on to vdW interactions. It has been shown that the $\nabla^2\rho(r_{CP})$ of conventional hydrogen bonds has a range of 0.578 to 0.843 $e^-\cdot Å^{-5}$.[36,37] By this measure, all heteropolar bonds in Table 1 show greater ionicity than conventional hydrogen bonds, whereas the homopolar one is a shared interaction in nature.

The dissociation energy (E_{BD}) for hydrogen bonds and their variants can be estimated from the potential energy density $V(r_{BCP})$ at the bond critical points, i.e., $E_{BD} = -(1/2)V(r_{BCP})$.[56,57] One way to calculate $V(r_{BCP})$ is by using the virial theorem, which relates the $V(r_{BCP})$ and the kinetic energy density $G(r_{BCP})$ to the local Laplacian $\nabla^2\rho(r_{BCP})$,

$$V(r_{CP}) = \frac{\hbar^2}{4m}\nabla^2\rho(r_{CP}) - 2G(r_{CP}) \quad (1)$$

For closed-shell interactions, a simple approach has been proposed for the evaluation of the $G(r_{BCP})$ from the experimental electron density distribution,[58]

$$G(r_{CP}) = \frac{3}{10}(3\pi^2)^{2/3}\rho^{5/3}(r_{CP}) + \frac{1}{6}\nabla^2\rho(r_{CP}) \quad (2)$$

This approximation was shown to yield a good agreement with the Hartree–Fock calculations[59] of $G(r_{BCP})$ in the medium-range region, i.e., 0.5–2.1 Å to the nuclei, where the chemical bonding usually takes place. As listed in Table 1, the leading N—H$^{\delta+}$···$^{\delta-}$H—B bonds (1.60 Å) in the *Ama*2 structure has the highest E_{BD} of 31.367 kJ·mol^{-1} (about 7% of the E_{BD} for a H_2 molecule), representing the strongest intermolecular interactions in this structure. These bonds are responsible for stabilizing the eclipsed molecules in the slabs. The secondary N—H$^{\delta+}$···$^{\delta-}$H—B bonds (1.96 Å) and the homopolar B—H$^{\delta-}$···$^{\delta-}$H—B bonds (2.03 Å) are inherently weaker, but still very important as they help to hold the slabs together. All three N—H$^{\delta+}$···$^{\delta-}$H—B bonds in the $Cmc2_1$ structure are significantly weaker than the intraslab N—H$^{\delta+}$···$^{\delta-}$H—B bonds in the *Ama*2 structure, which appear to be a reason why the latter is thermodynamically more stable. An additional advantage of the shorter bond length is that it yields a higher packing efficiency, or a smaller crystal volume (see Figure S3 in the SI). From

dx.doi.org/10.1021/jp509633h | J. Phys. Chem. C 2014, 118, 29591–29598

ambient pressure to 100 GPa, the volume of the *Ama*2 structure falls in the range of 96.2%−97.1%, to that of the *Cmc*21 structure, which makes the former energetically more favorable by virtue of a smaller *p*V work.

To characterize the homopolar dihydrogen interaction, we can extract a tail-to-tail $(NH_3BH_3)_2$ dimer from the *Ama*2 structure (Figure 5a). The two NH_3BH_3 molecules are linked by a B—$H^{\delta-}$···$^{\delta-}$H—B interaction, which, in the crystal, belong to two adjacent slabs. In this geometry, the two hydrogen atoms are equivalent (indicated as H_a and H_b). The calculated NBO charges on both H_a and H_b are −0.021 e^-, indicating a weak, shared interaction presenting between them. The calculated $\rho(r_{BCP})$ and $\nabla^2\rho(r_{BCP})$ at the bond critical point between H_a and H_b are 0.114 $e^-\cdot Å^{-3}$ and 1.35 $e^-\cdot Å^{-5}$, respectively; both are comparable to the corresponding values in the solid (Table 1). The calculated WBI value at the bond critical point is low, i.e., 0.012, which is also consistent with a weak, shared interaction.[24] This secondary B—$H^{\delta-}$···$^{\delta-}$H—B interaction is different from the charge transfer character of the heteropolar N—$H^{\delta+}$···$^{\delta-}$H—B interaction. For comparison, we can separate a head-to-tail $(NH_3BH_3)_2$ dimer from the same slab in the *Ama*2 structure (Figure 5b). For this dimer, the calculated amount of charge transfer in the N—$H^{\delta+}$···$^{\delta-}$H—B bond is *c.* −0.033 e^-, which is revealed in the NBO analysis as a more negatively charged H_b, compared to the other two H atoms bonded to the same B atom, and a more electron deprived H_a, compared to the other H atoms bonded to the same N atom. The same analysis revealed no evidence of charge transfer in the homopolar interaction for the tail-to-tail dimer.

The overlap population between two molecular fragments provides information on the nature of the interaction between the two fragmental orbitals; that is, positive and negative overlaps correspond to bonding (in-phase) and antibonding (out-of-phase) interactions, respectively. The CDA calculated overlap populations between the two NH_3BH_3 molecules in the tail-to-tail dimer are 0.072, 0.040, −0.009, and −0.165 for molecular orbitals (MO) #15, #16, #17, and #18, respectively. These results clearly reveal that orbitals #15 and #17 are bonding MOs, and orbitals #16 and #18 are their antibonding counterparts; an ECDA molecular orbital diagram is shown in Figure 6. The MO pair #15 and #16 is primarily derived from interactions between the fragmental orbital (#8) of the NH_3BH_3 monomers, while the pair #17 and #18 is primarily constructed by the fragmental orbital #9. In both cases, the MOs are dominated by the H—B pπ orbital with a larger lobe on the B atoms. Therefore, the B—$H^{\delta-}$···$^{\delta-}$H—B bond is the result of a secondary interaction of B—H bonds between the monomers. The calculated seconder order interaction energy (E^2) is 0.78 kcal/mol, which indicates a relatively weak interaction, but stronger than usually anticipated.

CONCLUSIONS

As a potential hydrogen storage material, NH_3BH_3 has received extensive scientific investigation over the past decades. The NH_3BH_3 molecules adopt a staggered conformation, which, in crystalline structures, are stabilized by the charge-transfer N—$H^{\delta+}$···$^{\delta-}$H—B interactions. In this article, we predicted the unprecedented eclipsed conformer to exist in the solid state of NH_3BH_3 under high pressure. A novel hydrogen−hydrogen interaction facilitated by hydrogen atoms with the same polarity, namely the homopolar B—$H^{\delta-}$···$^{\delta-}$H—B interaction, was also revealed in the solid state, which, surprisingly, may have the strength comparable to that of conventional hydrogen

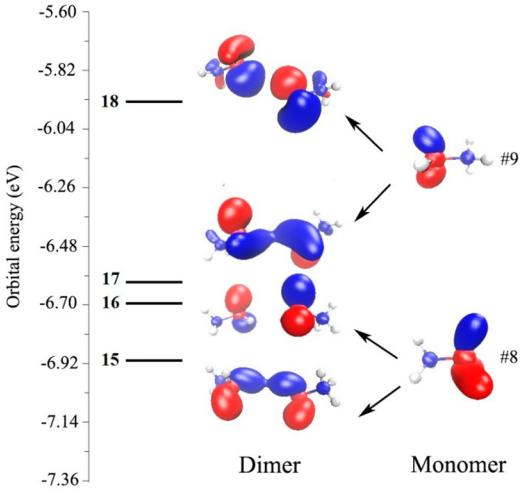

Figure 6. Molecular orbital diagram calculated for the homopolar B—$H^{\delta-}$···$^{\delta-}$H—B bond in a tail-to-tail $(NH_3BH_3)_2$ dimer extracted from the *Ama*2 structure (optimized at 10 GPa). The orbitals were plotted using an isovalue of 0.04 $e^-/Å^3$.

bonds. The B—$H^{\delta-}$···$^{\delta-}$H—B interaction originates from the secondary interactions between two BH_3 groups, in which the electron density is shared symmetrically between the participating H atoms. This bonding mechanism is distinctly different from the ubiquitous N—$H^{\delta+}$···$^{\delta-}$H—B interaction where electron donor and acceptor can be clearly identified. In the high-pressure crystalline structures, the B—$H^{\delta-}$···$^{\delta-}$H—B interaction has determining influences on crystal packing, which helps to stabilize the otherwise unfavorable eclipsed molecules. The results presented in this article represent an important advance in the understanding of ammonia borane, and dihydrogen interactions in general. The dihydrogen interactions potentially have the ability to assist in the release of molecular H_2 from solid structures, which may provide promising new routes to a rational design of hydrogen storage materials.

ASSOCIATED CONTENT

Supporting Information

Details of computed structural parameters for the predicted crystalline structures; a discussion of the predicted $P2_1/m$ structure; pressure dependences of the crystal volume and dihydrogen bond distances for NH_3BH_3 structures; phonon dispersions for the *Ama*2 and $P2_1/m$ structures; the experimentally observed $Cmc2_1$ and *Pnma* structures; and the Hirshfeld surface analysis of the *Ama*2 structure. This material is available free of charge via the Internet at http://pubs.acs.org.

AUTHOR INFORMATION

Corresponding Author

*E-mail: yansun.yao@usask.ca.

Notes

The authors declare no competing financial interest.

ACKNOWLEDGMENTS

Y.Y. thanks Dr. Joel Reid and Dr. Xia Liu for their insightful discussions. X.Y. acknowledges the financial support from the China Scholarship Council. All authors are grateful to the Information and Communications Technology group at the University of Saskatchewan for providing the Plato cluster computing resource, which is part of the High Performance

Computing Training and Research Facilities at the University of Saskatchewan. Part of the calculations have been performed through the use of the computing resources provided by WestGrid and Compute Canada. This project was supported by Natural Sciences and Engineering Research Council of Canada (NSERC).

REFERENCES

(1) Brown, M. P.; Heseltine, R. W. Co-ordinated BH_3 as a Proton Acceptor Group in Hydrogen Bonding. *Chem. Commun.* **1968**, 1551−1552.
(2) Richardson, T. B.; de Gala, S.; Crabtree, R. H.; Seigbhan, P. E. M. Unconventional Hydrogen Bonds: Intermolecular B—H···H—N Interactions. *J. Am. Chem. Soc.* **1995**, *117*, 12875−12876.
(3) Custelcean, R.; Jackson, J. E. Dihydrogen Bonding: Structures, Energetics, and Dynamics. *Chem. Rev.* **2001**, *101*, 1963−1980.
(4) Calhorda, M. J. Weak Hydrogen Bonds: Theoretical Studies. *Chem. Commun.* **2000**, 801−809.
(5) Shubina, E. S.; Belkova, N. V.; Epstein, L. M. Novel Types of Hydrogen Bonding with Transition Metal π-Complexes and Hydrides. *J. Organomet. Chem.* **1997**, *536*−*537*, 17−29.
(6) Bowden, M. E.; Gainsford, G. J.; Robinson, W. T. Room-Temperature Structure of Ammonia Borane. *Aust. J. Chem.* **2007**, *60*, 149−153.
(7) Allis, D. G.; Kosmowski, M. E.; Hudson, B. S. The Inelastic Neutron Scattering Spectrum of $H_3B{:}NH_3$ and the Reproduction of Its Solid-State Features by Periodic DFT. *J. Am. Chem. Soc.* **2004**, *126*, 7756−7757.
(8) Klooster, W. T.; Koetzle, T. F.; Siegbahn, P. E. M.; Richardson, T. B.; Crabtree, R. H. Study of the N—H···H—B Dihydrogen Bond Including the Crystal Structure of BH_3NH_3 by Neutron Diffraction. *J. Am. Chem. Soc.* **1999**, *121*, 6337−6343.
(9) Trudel, S.; Gilson, D. F. R. High-Pressure Raman Spectroscopic Study of the Ammonia−Borane Complex. Evidence for the Dihydrogen Bond. *Inorg. Chem.* **2003**, *42*, 2814−2816.
(10) Custelcean, R.; Dreger, Z. A. Dihydrogen Bonding under High Pressure: A Raman Study of BH_3NH_3 Molecular Crystal. *J. Phys. Chem. B* **2003**, *107*, 9231−9235.
(11) Lin, Y.; Mao, W. L.; Drozd, V.; Chen, J.; Daemen, L. L. Raman Spectroscopy Study of Ammonia Borane at High Pressure. *J. Chem. Phys.* **2008**, *129*, 234509.
(12) Kupenko, I.; Dubrovinsky, L.; Dmitriev, V.; Dubrovinskaia, N. In Situ Raman Spectroscopic Study of the Pressure Induced Structural Changes in Ammonia Borane. *J. Chem. Phys.* **2012**, *137*, 074506.
(13) Filinchuk, Y.; Nevidomskyy, A. H.; Chernyshov, D.; Dmitriev, V. High-Pressure Phase and Transition Phenomena in Ammonia Borane NH_3BH_3 from X-ray Diffraction, Landau Theory, and Ab Initio Calculations. *Phys. Rev. B* **2009**, *79*, 214111.
(14) Chen, J.; Couvy, H.; Liu, H.; Drozd, V.; Daemen, L. L.; Zhao, Y.; Kao, C.-C. In Situ X-ray Study of Ammonia Borane at High Pressures. *Int. J. Hydrogen Energy* **2010**, *35*, 11064−11070.
(15) Nylén, J.; Eriksson, L.; Benson, D.; Häussermann, U. Characterization of a High Pressure, High Temperature Modification of Ammonia Borane (BH_3NH_3). *J. Chem. Phys.* **2013**, *139*, 054507.
(16) Xie, S.; Song, Y.; Liu, Z. *In Situ* High-Pressure Study of Ammonia Borane by Raman and Infrared Spectroscopy. *Can. J. Chem.* **2009**, *87*, 1235−1247.
(17) Kumar, R. S.; Ke, X. Z.; Zhang, J. Z.; Lin, Z. J.; Vogel, S. C.; Hartl, M.; Sinogeikin, S.; Daemen, L.; Cornelius, A. L.; Chen, C. F.; Zhao, Y. S. Pressure Induced Structural Changes in the Potential Hydrogen Storage Compound Ammonia Borane: A Combined X-ray, Neutron and Theoretical Investigation. *Chem. Phys. Lett.* **2010**, *495*, 203−207.
(18) Wang, L.; Bao, K.; Meng, X.; Wang, X.; Jiang, T.; Cui, T.; Liu, B.; Zou, G. Structural and Dynamical Properties of Solid Ammonia Borane under High Pressure. *J. Chem. Phys.* **2011**, *134*, 024517.
(19) Liu, A.; Song, Y. In Situ High-Pressure and Low-Temperature Study of Ammonia Borane by Raman Spectroscopy. *J. Phys. Chem. C* **2012**, *116*, 2123−2131.
(20) Lin, Y.; Ma, H. W.; Matthews, C. W.; Kolb, B.; Sinogeikin, S.; Thonhauser, T.; Mao, W. L. Experimental and Theoretical Studies on a High Pressure Monoclinic Phase of Ammonia Borane. *J. Phys. Chem. C* **2012**, *116*, 2172−2178.
(21) Najiba, S.; Chen, J.; Drozd, V.; Durygin, A.; Sun, Y. Ammonia Borane at Low Temperature Down to 90 K and High Pressure up to 15 GPa. *Int. J. Hydrogen Energy* **2013**, *38*, 4628−4635.
(22) Bader, R. F. W. *Atoms in Molecules—A Quantum Theory*; Oxford University Press: Oxford, 1990.
(23) Weinhold, F.; L, C. R. *Discovering Chemistry with Natural Bond Orbitals*. John Wiley & Sons: New York, 2012.
(24) Wiberg, K. Application of the Pople-Santry-Segal CNDO Method to the Cyclopropylcarbinyl and Cyclobutyl Cation and to Bicyclobutane. *Tetrahedron* **1968**, *24*, 1083−1096.
(25) Frenking, G.; Fröhlich, N. The Nature of the Bonding in Transition-Metal Compounds. *Chem. Rev.* **2000**, *100*, 717−774.
(26) Flacau, R.; Yao, Y.; Klug, D. D.; Desgreniers, D.; Ratcliffe, C. I. Structural Phase Transitions Induced by Pressure in Ammonium Borohydride. *Phys. Chem. Chem. Phys.* **2012**, *14*, 7005−7011.
(27) Yao, Y.; Hoffmann, R. BH_3 under Pressure: Leaving the Molecular Diborane Motif. *J. Am. Chem. Soc.* **2011**, *133*, 21002−21009.
(28) Kresse, G.; Hafner, J. Ab Initio Molecular Dynamics for Liquid Metals. *Phys. Rev. B* **1993**, *47*, 558−561.
(29) Blöchl, P. E. Projector Augmented-Wave Method. *Phys. Rev. B* **1994**, *50*, 17953−17979.
(30) Kresse, G.; Joubert, D. From Ultrasoft Pseudopotentials to the Projector Augmented-Wave Method. *Phys. Rev. B* **1999**, *59*, 1758−1775.
(31) Perdew, J. P.; Burke, K.; Ernzerhof, M. Generalized Gradient Approximation Made Simple. *Phys. Rev. Lett.* **1996**, *77*, 3865−3868.
(32) Gonze, X.; Beuken, J.-M.; Caracas, R.; Detraux, F.; Fuchs, M.; Rignanese, G.-M.; Sindic, L.; Verstraete, M.; Zerah, G.; Jollet, F.; et al. First-Principles Computation of Material Properties: the ABINIT Software Project. *Comput. Mater. Sci.* **2002**, *25*, 478−492.
(33) Troullier, N.; Martins, J. Efficient Pseudopotentials for Plane-Wave Calculations. *Phys. Rev. B* **1991**, *43*, 1993−2006.
(34) Krack, M. Pseudopotentials for H to Kr Optimized for Gradient-Corrected Exchange-Correlation Functionals. *Theor. Chem. Acc.* **2005**, *114*, 145−152.
(35) Katan, C.; Rabiller, P.; Lecomte, C.; Guezo, M.; Oison, V.; Souhassou, M. Numerical Computation of Critical Properties and Atomic Basins from Three-Dimensional Grid Electron Densities. *J. Appl. Crystallogr.* **2003**, *36*, 65−73.
(36) Koch, U.; Popelier, P. L. A. Characterization of C—H—O Hydrogen Bonds on the Basis of the Charge Density. *J. Phys. Chem.* **1995**, *99*, 9747−9754.
(37) Popelier, P. L. A. Characterization of a Dihydrogen Bond on the Basis of the Electron Density. *J. Phys. Chem. A* **1998**, *102*, 1873−1878.
(38) Tse, J. S.; Yao, Y.; Klug, D. D.; Desgreniers, S. Bonding in the ε-Phase of High Pressure Oxygen. *J. Phys.: Conf. Ser.* **2008**, *121*, 012006.
(39) Frisch, M. J.; Trucks, G. W.; Schlegel, H. B.; Scuseria, G. E.; Robb, M. A.; Cheeseman, J. R.; Scalmani, G.; Barone, V.; Mennucci, B.; Petersson, G. A.; Nakatsuji, H.; Caricato, M.; Li, X.; Hratchian, H. P.; Izmaylov, A. F.; Bloino, J.; Zheng, G.; Sonnenberg, J. L.; Hada, M.; Ehara, M.; Toyota, K.; Fukuda, R.; Hasegawa, J.; Ishida, M.; Nakajima, T.; Honda, Y.; Kitao, O.; Nakai, H.; Vreven, T.; Montgomery, J. A., Jr.; Peralta, J. E.; Ogliaro, F.; Bearpark, M.; Heyd, J. J.; Brothers, E.; Kudin, K. N.; Staroverov, V. N.; Kobayashi, R.; Normand, J.; Raghavachari, K.; Rendell, A.; Burant, J. C.; Iyengar, S. S.; Tomasi, J.; Cossi, M.; Rega, N.; Millam, J. M.; Klene, M.; Knox, J. E.; Cross, J. B.; Bakken, V.; Adamo, C.; Jaramillo, J.; Gomperts, R.; Stratmann, R. E.; Yazyev, O.; Austin, A. J.; Cammi, R.; Pomelli, C.; Ochterski, J. W.; Martin, R. L.; Morokuma, K.; Zakrzewski, V. G.; Voth, G. A.; Salvador, P.; Dannenberg, J. J.; Dapprich, S.; Daniels, A. D.; Farkas, O.;

Foresman, J. B.; Ortiz, J. V.; Cioslowski, J.; Fox, D. J. *Gaussian 09*; Gaussian, Inc.: Wallingford, CT, 2009.
(40) Lu, T.; Chen, F. Multiwfn: A Multifunctional Wavefunction Analyzer. *J. Comput. Chem.* **2012**, *33*, 580−592.
(41) Momma, K.; Izumi, F. *VESTA 3* for Three-Dimensional Visualization of Crystal, Volumetric and Morphology Data. *J. Appl. Crystallogr.* **2011**, *44*, 1272−1276.
(42) Humphrey, W.; Dalke, A.; Schulten, K. VMD: Visual Molecular Dynamics. *J. Mol. Graphics* **1996**, *14*, 33−38.
(43) Mo, Y.; Song, L.; Wu, W.; Zhang, Q. Charge Transfer in the Electron Donor−Acceptor Complex BH_3NH_3. *J. Am. Chem. Soc.* **2004**, *126*, 3974−3982.
(44) Bader, R. F. W.; MacDougall, P. J.; Lau, C. D. H. Bonded and Nonbonded Charge Concentrations and Their Relation to Molecular Geometry and Reactivity. *J. Am. Chem. Soc.* **1984**, *106*, 1594−1605.
(45) Cremer, D.; Kraka, E. Chemical Bonds without Bonding Electron Density—Does the Difference Electron-Density Analysis Suffice for a Description of the Chemical Bond? *Angew. Chem., Int. Ed.* **1984**, *23*, 627−628.
(46) Song, Y. New Perspectives on Potential Hydrogen Storage Materials using High Pressure. *Phys. Chem. Chem. Phys.* **2013**, *15*, 14524−14547.
(47) Clayden, J.; Greeves, N.; Warren, S. *Organic Chemistry*; Oxford University Press: Oxford, 2012.
(48) Grochala, W.; Hoffmann, R.; Feng, J.; Ashcroft, N. W. The Chemical Imagination at Work in Very Tight Places. *Angew. Chem., Int. Ed.* **2007**, *46*, 3620−3642.
(49) Cramer, C. J.; Gladfelter, W. L. Ab Initio Characterization of $[H_3N{\cdot}BH_3]_2$, $[H_3N{\cdot}AlH_3]_2$, and $[H_3N{\cdot}GaH_3]_2$. *Inorg. Chem.* **1997**, *36*, 5358−5362.
(50) Matta, C. F. In: *Hydrogen Bonding-New Insights*; Grabowski, S. J., Ed.; Springer: New York, 2006; Chapter 9.
(51) Guerra, D.; David, J.; Restrepo, A. $(H_3N{-}BH_3)_4$: The Ammonia Borane Tetramer. *Phys. Chem. Chem. Phys.* **2012**, *14*, 14892−14897.
(52) Wolstenholme, D. J.; Traboulsee, K. T.; Hua, Y.; Calhoun, L. A.; McGrady, G. S. Thermal Desorption of Hydrogen from Ammonia Borane: Unexpected Role of Homopolar N—H···H—B Interactions. *Chem. Commun.* **2012**, *48*, 2597−2599.
(53) Wolstenholme, D. J.; Titah, J. T.; Che, F. N.; Traboulsee, K. T.; Flogeras, J.; McGrady, G. S. Homopolar Dihydrogen Bonding in Alkali-Metal Amidoboranes and Its Implications for Hydrogen Storage. *J. Am. Chem. Soc.* **2011**, *133*, 16598−16604.
(54) Novoa, J. J.; Whangbo, M.-H. Interactions Energies Associated with Short Intermolecular Contacts of C—H Bonds. II. *Ab Initio* Computational Study of the C—H···H—C Interactions in Methane Dimer. *J. Chem. Phys.* **1991**, *94*, 4835−4841.
(55) Echeverría, J.; Aullon, G.; Danovich, D.; Shaik, S.; Alvarez, S. Dihydrogen Contacts in Alkanes Are Subtle But Not Faint. *Nat. Chem.* **2011**, *3*, 323−330.
(56) Souhassou, M.; Lecomte, C.; Ghermani, N.-E.; Rohmer, M. M.; Wiest, R.; Benard, M.; Blessing, R. H. Electron Distributions in Peptides and Related Molecules. 2. An Experimental and Theoretical Study of (Z)-*N*-Acetyl-α,β-dehydrophenylalanine Methylamide. *J. Am. Chem. Soc.* **1992**, *114*, 2371−2382.
(57) Espinosa, E.; Molins, E.; Lecomte, C. Hydrogen Bond Strengths Revealed by Topological Analyses of Experimentally Observed Electron Densities. *Chem. Phys. Lett.* **1998**, *285*, 170−173.
(58) Abramov, Yu. A. On the Possibility of Kinetic Energy Density Evaluation from the Experimental Electron-Density Distribution. *Acta Crystallogr.* **1997**, *A53*, 264−272.
(59) Bader, R. F. W.; Essén, H. The Characterization of Atomic Interactions. *J. Chem. Phys.* **1984**, *80*, 1943−1960.